Science of the Total Environment 788 (2021) 147579

Contents lists available at ScienceDirect

Science of the Total Environment

journal homepage: www.elsevier.com/locate/scitotenv

Release of trace elements during bioreductive dissolution of magnetite from metal mine tailings: Potential impact on marine environments

Jordi Palau [a,b,*], Robert Benaiges-Fernandez [a,b], Francesco Offeddu [a], Jordi Urmeneta [b,c], Josep M. Soler [a], Jordi Cama [a], Bernhard Dold [d,e]

[a] Institute of Environmental Assessment and Water Research (IDAEA), CSIC, Barcelona 08034, Catalonia, Spain
[b] University of Barcelona, Barcelona 08028, Catalonia, Spain
[c] Biodiversity Research Institute (IRBio), University of Barcelona, Barcelona 08028, Catalonia, Spain
[d] Pontifical Catholic University of Peru (PUCP), San Miguel, Lima, Peru
[e] SUMIRCO, San Pedro de la Paz, Chile

HIGHLIGHTS

- High contents of TEs were detected in magnetite from the tailings and ore samples.
- Fe(III) bioreduction of magnetite was observed under marine sediment conditions.
- Several TEs such as Mn, V, As and Cu were released to the aqueous phase.
- Potential TEs pollution of sediment and pore water by submarine tailings disposal.
- The results can help to better evaluate the impact of submarine tailings disposal.

GRAPHICAL ABSTRACT

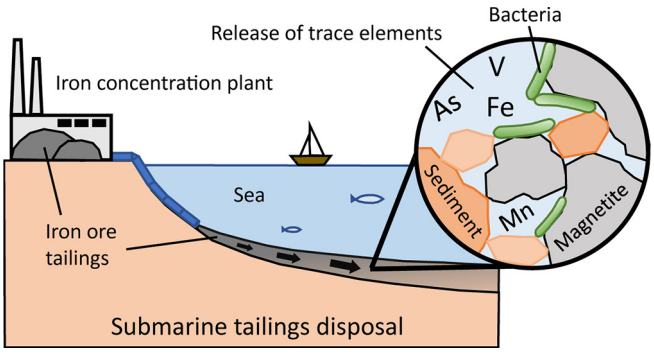

ARTICLE INFO

Article history:
Received 7 March 2021
Received in revised form 1 May 2021
Accepted 2 May 2021
Available online 7 May 2021

Editor: Damia Barcelo

Keywords:
Marine pollution
Mining contamination
Submarine tailings disposal
Dissimilatory metal-reducing bacteria
Shewanella loihica

ABSTRACT

Adverse impacts of mine tailings on water and sediments quality are major worldwide environmental problems. Due to the environmental issues associated with the deposition of mine tailings on land, a controversial discussed alternative is submarine tailings disposal (STD). However, Fe(III) bioreduction of iron oxides (e.g., magnetite) in the tailings disposed might cause toxic effects on coastal environments due to the release of different trace elements (TEs) contained in the oxides.

To study the extent and kinetics of magnetite bioreduction under marine conditions and the potential release of TEs, a number of batch experiments with artificial seawater (pH 8.2) and a marine microbial strain (*Shewanella loihica*) were performed using several magnetite ore samples from different mines and a mine tailings sample. The elemental composition of the magnetite determined in the tailings showed relatively high amounts of TEs (e.g., Mn, Zn, Co) compared with those of the magnetite ore samples (LA-ICP-MS and EMPA analyses). The experiments were conducted at 10 °C in the dark for up to 113 days. Based on the consumption of lactate and production of acetate and aqueous Fe(II) over time, the magnitude of Fe(III) bioreduction was calculated using a geochemical model including Monod kinetics. Model simulations reproduced the release of iron and TEs observed throughout the experiments, e.g., Mn (up to 203 μg L^{-1}), V (up to 79 μg L^{-1}), As (up to 17 μg L^{-1}) and Cu (up to 328 μg L^{-1}), suggesting a potential contamination of pore water by STD. Therefore, the results of this study can help to better evaluate the potential impacts of STD.

* Corresponding author at: Grup MAiMA, SGR Mineralogia Aplicada, Geoquímica i Geomicrobiologia, Departament de Mineralogia, Petrologia i Geologia Aplicada, Facultat de Ciències de La Terra, Universitat de Barcelona (UB), 08028 Barcelona, Catalonia, Spain.
E-mail address: jordi.palau@ub.edu (J. Palau).

https://doi.org/10.1016/j.scitotenv.2021.147579

1. Introduction

Adverse impacts of metal mine tailings on water and sediment quality are a major environmental problem (Lottermoser, 2010; Younger et al., 2002). Due to the known environmental issues associated with mine tailings deposition on land (e.g., acid mine drainage (Dold, 2014a) and tailings dam failures (Buch et al., 2021; Rico et al., 2008)), alternatives for tailings management such as submarine tailings disposal (STD) are being considered and used in some countries such as Norway and Chile (Dold, 2014b; Ramirez-Llodra et al., 2015). However, severe ecological impacts of STD on active and historical sites were reported worldwide (Dold, 2014b; Hughes et al., 2015; Morello et al., 2016; Ramirez-Llodra et al., 2015).

In addition to the physical impacts of STD on the seafloor biota due to massive tailings discharge and extremely high sedimentation rates (i.e., hyper-sedimentation) (Morello et al., 2016; Ramirez-Llodra et al., 2015), toxic effects may occur due to heavy metals (e.g., V, Cu, Zn, Ni, Pb, Cr, Cd etc.) and metalloids (e.g., As) release (Dold, 2014b; Koski, 2012; Morello et al., 2016; Ramirez-Llodra et al., 2015). Most of the field studies on marine environments contamination by metal(loid)s from mining activities investigated sites impacted by sulfide ore tailings (Angel et al., 2013; Dold, 2014b; Gambi et al., 2020; Koski, 2012; Pedersen et al., 2018; Sternal et al., 2017). Recent laboratory studies also investigated the potential impacts of metal sulfide minerals and sulfide-containing tailings to marine environments (Embile Jr. et al., 2018; Simpson and Spadaro, 2016).

However, iron oxide minerals such as magnetite and hematite can also contain high amounts of environmental hazardous trace elements (TEs) (Nystrom and Henriquez, 1994) and contribute to metal contamination of marine sediment and pore water by reductive dissolution, even during sulfide ore tailings disposal (Dold, 2014b). For instance, Pb—Zn ore tailings directly released to the Mediterranean Sea between 1957 and 1990 in Portman Bay (Spain) contained an iron oxides (magnetite, hematite and goethite) concentration of 15.6% (mineral treated during 1973, Manteca et al., 2014). Nowadays, as far as we know, there are two operations in Norway (for one of them the latest production period lasted from 2009 to 2015) and one in Chile which deposit iron oxide ore (mainly magnetite) tailings in submarine environments (Dold, 2014b; Ramirez-Llodra et al., 2015; Trannum et al., 2018). Given the enormous amounts of iron ore tailings released to the sea, the liberation of iron, a limiting nutrient for phytoplankton production (Boyd et al., 2000; Dold et al., 2013), during Fe(III) bioreduction might enhance the risk of eutrophication and deoxygenation of the marine environment.

In order to address the potential environmental impact of the submarine deposition of iron oxide containing mine tailings, we present a study in which batch experiments were performed using a number of magnetite ore samples from Chilean and Swedish mines and a mine tailings sample. The main goal was to investigate the extent and the kinetics of iron ore minerals bioreduction under marine conditions and the potential release of TEs to the aqueous phase. The magnitude of microbial reduction of Fe(III) was evaluated using a geochemical model including Monod kinetics.

In most of the samples investigated in this study, iron oxides are mainly composed of magnetite ($Fe^{2+}Fe_2^{3+}O_4$), which is an iron ore (Knipping et al., 2015; Nystrom and Henriquez, 1994) (72.36% Fe) and a common mineral in sulfide ore bodies and their host rocks (Boutroy et al., 2014; Makvandi et al., 2016; Nadoll et al., 2014). Magnetite forms under a wide variety of geologic conditions and a large range of minor and TEs can be incorporated in its spinel structure (Boutroy et al., 2014; Dare et al., 2014; Makvandi et al., 2016; Nadoll et al., 2015, 2014). For instance, cations such as Mn, Zn, Ni and Co may substitute Fe^{2+}, whereas others like Al, Cr, V and Ga can replace Fe^{3+} sites (Makvandi et al., 2016; Nadoll et al., 2014). As a result, elements such as Al, Ti, V, Cr, Mn, Co, Ni, Zn and Ga are commonly present in magnetite at concentrations from 10 to >1000 mg Kg^{-1} (Nadoll et al., 2014). Given the potential amounts of TEs in magnetite, STD of magnetite-bearing mine tailings could adversely affect the marine environment by TEs contamination.

The magnitude of the impact on marine biota depends on the amount of metal that is bioavailable. Dissolved species and free metal cations are considered the most bioavailable forms (Morello et al., 2016; Ramirez-Llodra et al., 2015; Simpson and Spadaro, 2016). In sediments where reducing conditions prevail, iron oxides may be affected by microbial reductive dissolution (Kappler and Straub, 2005; Lovley et al., 2004), which can lead to TEs release into the aqueous phase (Ribet et al., 1995; Zachara et al., 2001). A recent study investigated the leaching of metals from iron ore tailings under different pH and low-molecular-weight organic acids (Geng et al., 2020). However, the conditions and/or metal oxides investigated in previous studies are different than those in natural marine environments impacted by iron oxides from mine tailings. In contrast to iron oxides, sulfide minerals are relatively stable under anoxic conditions (Dold, 2014b; Morello et al., 2016). Trace metal release and bioavailability will thus depend on the properties and characteristics of the metal and host mineral(s) as well as on the geochemical conditions of the STD site. Therefore, further research on potential TEs release from iron oxide ores such as magnetite under conditions closer to marine environments is needed for the assessment of environmental impacts associated with STD.

2. Materials and methods

2.1. Solid samples

The solids used for the experiments were seven iron ore samples, one iron ore tailings sample and four synthetic monomineralic samples. Five iron ore samples were from different mines in Chile (C1 to C5-T) and two samples from Swedish mines (S1 and S2) (Table S1 in the Supplementary Material (SM)). Since these mine samples were from iron ore deposits formed under different geological conditions, variations in TEs composition of the iron oxides were expected (Nadoll et al., 2014). Ore subsamples were crushed to powder fractions between 60 and 100 μm and subsequently homogenized prior to use in the experiments and analyses. The iron oxide ore tailings sample was collected at the iron concentration plant (80th percentile value of 44 μm) of the mine from where the C5-T sample was extracted (see details in SM).

As for the monomineralic samples, synthetic ferrihydrite 2-Line ($Fe_5^{3+}HO_8 \cdot 4H_2O$, particle size <60 μm) was produced in the laboratory according to Schwertmann and Cornell (2000) (i.e., F sample), whereas synthetic powder (<5 μm) samples of magnetite ($Fe^{2+}Fe_2^{3+}O_4$), hematite ($Fe_2^{3+}O_3$) and goethite ($Fe^{3+}O(OH)$) were purchased from Sigma-Aldrich (i.e., M, H and G, respectively).

2.2. Solid characterization

Samples were analyzed using X-ray diffraction (XRD) analysis and Rietveld refinement (Bish and Howard, 1988), scanning electron microscopy (SEM) and energy dispersive X-ray spectrometry (EDS), electron microprobe analysis (EMPA) and laser ablation inductively coupled plasma mass spectrometry (LA-ICP-MS). Details on the equipment and settings used are available in SM (Sections 1, 2 and Table S2). For the iron ore samples, the mineralogical study indicated that, except for C4 sample with about 40 wt% of hematite, the metal oxides fraction was composed of magnetite with amounts ranging from approximately 90 to <5 wt% (see Table S1 in SM). This wide range covers well the content of iron oxides in sediments impacted by STD in active and historical sites. In some samples, other major constituents (>10 wt%) are silicates (amphibole, chlorite and plagioclase) and phosphates (apatite-(CaOH)). In the C3 sample, there is a substantial amount of chalcopyrite ($CuFeS_2$, ≈13 wt%) (Table S1 in SM). The tailings sample is mainly composed of gangue minerals, primarily silicates (amphibole, chlorite, plagioclase and talc), plus a minor amount (<5 wt%) of unrecoverable

iron oxide minerals (mainly magnetite). The XRD analyses showed that the commercial and synthesized samples were composed of the respective iron (hydr)oxides and the lack of minor phases. The specific surface area of all samples was determined by the Brunauer-Emmett-Teller (BET) method (Brunauer et al., 1938) (Table S1 in SM).

Quantitative elemental analyses of the iron oxide minerals and other phases in the tailings and iron oxide ore samples were performed by EMPA and LA-ICP-MS. Bulk sample elemental composition was determined by total acid digestion and ICP analysis.

2.3. Batch experiments

For the Fe(III) bioreduction experiments with iron (hydr)oxides, a marine bacterium *Shewanella loihica* PV-4 (Gao et al., 2006; Roh et al., 2006) was used as a model microorganism (cultivation details in SM). *Shewanella loihica* is capable to grow under both oxic and anoxic conditions using oxygen or ferric iron as terminal electron acceptor (TEA), respectively (Gao et al., 2006; Roh et al., 2006). Fifty-five glass tubes of 25 mL nominal volume (15 cm long × 1.5 cm internal diameter) were used for the microcosms (5 tubes for each solid sample) and 33 tubes for the abiotic controls (3 tubes for each solid). 0.25 g of powder sample were placed in each tube, which were subsequently filled with artificial seawater (ASW) under atmospheric conditions (preparation details in SM). ASW was amended with sodium lactate (10 mM) as electron donor and carbon source and ammonium chloride (1.87 mM) as a source of nitrogen. Tris(hydroxymethyl)aminomethane hydrochloride (TRIS-HCl, 10 mM) was used as a pH-buffer and the ASW solution was adjusted to pH of 8.2 with 1 N NaOH solution. In contrast to nutrient-rich solutions, the minimal growth medium used in this study may better represent the conditions in STD sites. No exogenous electron carrier substances (e.g., anthraquinone-2,6-disulfonate, AQDS) or reducing agents (e.g., cysteine) were added to the solution.

Except for the abiotic controls, *S. loihica* was aseptically inoculated into the tubes containing the medium and the solid previously sterilized (preparation details in SM) to a final number of ~$1 \cdot 10^7$ colony-forming units (cfu) mL^{-1} (measured by agar culture, LB). The microcosms and abiotic controls were tightly closed using closed-top screw caps with butyl liner and sealed with Parafilm M. A minimal headspace was left to avoid cracking of the tubes due to overpressure.

Thereafter, all tubes were stirred for ~15 s by a vortex mixer and immediately placed horizontally for incubation into a thermostatic water bath at 10 ± 1 °C without agitation in the dark until sampled. The relatively low incubation temperature and the static conditions were selected to be similar to marine sediment environments in STD sites. The horizontal disposition allowed the solid to settle down in a thin layer (thickness ≤ 1 mm) over the side of the tubes. The relatively small solid/liquid ratio (approximately 9.5 g L^{-1}) and the horizontal disposition of the tubes were intended to maximize the solid–liquid contact. Additional abiotic controls were prepared under anoxic conditions using degassed (O_2-free) water, either ASW or Milli-Q water (experimental details in SM).

The experiments lasted 113 days in order to investigate the progress of Fe(III) bioreduction and the processes that may control its rate, extent and the potential release of TEs to the aqueous phase. Microcosms and controls were removed from the thermostatic bath at different times and placed immediately in the anoxic glovebox for sampling. The liquid was collected to measure the concentrations of lactate and acetate (high performance liquid chromatography (HPLC)) and metal(loid)s (ICP coupled to optical emission spectroscopy (ICP-OES) and ICP-MS). Uncertainties were estimated based on the analysis of sample replicates with different concentrations (details in SM). Measurements of dissolved iron speciation were performed by phenanthroline colorimetry. The solution pH, Eh and dissolved oxygen (DO) concentration were also measured. The solid was retrieved and preserved for XRD-Rietveld analysis, Field Emission SEM-EDS and Attenuated Total Reflectance-Fourier Transform Infrared Spectroscopy (ATR-FTIR). Further information on the analytical techniques, sampling and samples preservation is provided in the SM.

2.4. Geochemical modeling

The variation in the concentrations of lactate, acetate and the release of iron and TEs during the batch experiments were simulated by a kinetic model developed with the PHREEQC code (Parkhurst and Appelo, 1999) and the wateq4f.dat thermodinamic database. A Monod kinetic rate expression for substrate (i.e., lactate) utilization coupled to cell growth was used (Liu et al., 2001b; Watson et al., 2003). Monod kinetic equations allow to describe the competitive use of different TEAs (e.g., dissolved oxygen, Mn(IV), Fe(III), etc.) by the bacteria:

$$r = \frac{dS}{dt} = -k_{max} \cdot X \cdot \frac{S}{K_S + S} \cdot \frac{TEA}{K_{TEA} + TEA} \cdot \frac{K_{In}}{K_{In} + In} \quad (1)$$

where r is the rate of consumption of substrate S (mol L^{-1} s^{-1}), k_{max} is the maximum substrate consumption rate (s^{-1}), X, S, TEA and In are the concentration of the cell biomass, substrate, particular TEA and inhibiting substance (mol L^{-1}), respectively, K_S and K_{TEA} are the Monod half-saturation constants with respect to S and TEA (mol L^{-1}), respectively, and K_{In} corresponds to the respective inhibition constant (mol L^{-1}). For instance, under reducing conditions, magnetite bioreduction in the experiments performed in this study could be expressed as:

$$C_3H_5O_3^- + 0.15\ NH_4^+ + 1.5\ Fe^{2+}Fe^{3+}{}_2O_4 + 8.35H^+ \rightarrow 0.75\ C_2H_3O_2^- + 0.75\ HCO_3^- + 0.15\ C_5H_7O_2N + 4.5\ Fe(II) + 4.95\ H_2O \quad (2)$$

where $C_3H_5O_3^-$ and $C_2H_3O_2^-$ are lactate and acetate, respectively. A cell biomass formula of $C_5H_7O_2N$ was assumed according to previous studies (Maier, 2009; Roden and Jin, 2011) to convert measurements of cfu to moles of cell biomass (see SM, Section 7). Cell biomass changes (e.g., growth or decay) during the experiment were simulated by a simple model that includes first-order decay rate (Thullner et al., 2007, 2005):

$$\frac{dX}{dt} = Y \cdot r - \mu_{dec} \cdot X \cdot In_{dec} \quad (3)$$

where r is the rate of substrate consumption from Eq. (1), Y is the molar biomass yield, such that Y = mol of biomass (i.e., $C_5H_7O_2N$) produced/mol of substrate (i.e., $C_3H_5O_3^-$) consumed, and μ_{dec} is the decay rate coefficient (s^{-1}). An inhibition factor, $In_{dec} = 1 - (X_{min}/X)$, which inhibits the decay at low cell concentrations (i.e., X_{min}) was used (Table S4 in SM). Microbial growth was simulated by including biomass (i.e., $C_5H_7O_2N$) as a product in the reaction stoichiometries (e.g., Eq. (2)) according to Y, which requires different reaction stoichiometries for different values of Y.

Details on the parameters used in Eqs. (1) and (3) and the stoichiometric coefficients of the reactions simulated with PHREEQC (Eq. (2)) are available in the SM (Tables S3 and S4). A potential formation of secondary minerals (magnetite and/or siderite ($Fe^{2+}CO_3$)) by reaction of produced Fe(II) (Eq. (2)) with iron (hydr)oxides or anions in solution, respectively, was considered in the calculations (Eqs. (S2) and (S3) in SM). In Eq. (2), magnetite is assumed to be stoichiometric (i.e., $Fe^{2+}/Fe^{3+} = 0.5$). However, as partially oxidized magnetite ($Fe^{2+}/Fe^{3+} < 0.5$, commonly referred to as non-stoichiometric magnetite) is also possible (Usman et al., 2018), a non-stoichiometric magnetite was also utilized in the simulations (see Section 3.3). Throughout the manuscript, the notations "Fe(II)" and "Fe^{2+}" generally refer to dissolved ferrous iron species and structural ferrous iron, respectively.

3. Results and discussion

3.1. Geochemical composition of iron oxides

The TEs content of magnetite in C1, C2, C3, S1, S2 and CT samples measured by in-situ LA-ICP-MS is illustrated in Fig. 1. For the C4 sample, with approximately 40 wt% of hematite (Table S1 in SM), the TEs composition of hematite is shown in Fig. S1 in SM. The elemental composition of the C5-T sample was determined by EMPA and total acid digestion. LA-ICP-MS elemental compositions of magnetite from ore samples of the same mine are available in the literature and were used for comparison (Knipping et al., 2015).

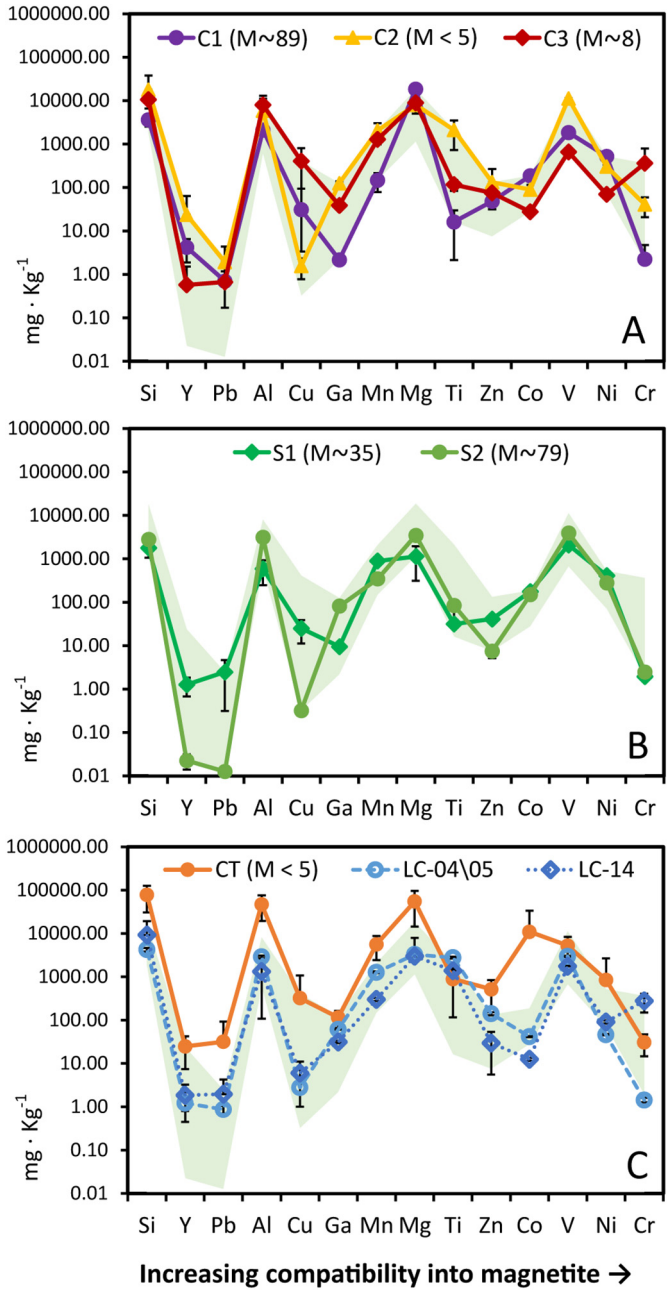

Fig. 1. Trace element content (mg kg^{-1}) of magnetite determined by LA-ICP-MS in this study and from the literature. A) Samples from Chilean deposits: C1 and C2 are from Iron Oxide Apatite (IOA) deposits and C3 is from an Iron Oxide Cupper Gold (IOCG) deposit. B) Samples S1 and S2 are from iron IOA-type deposits in Sweden. C) Iron ore tailings sample (CT) obtained at the outlet of a plant that processes magnetite ore from an IOA-type deposit. Data of ore samples from the same deposit, from a magnetite dike (LC-04\05) and an adjacent brecciated diorite intrusion (LC-14), available in the literature were also illustrated (Knipping et al., 2015). The shaded area corresponds to the range of average concentrations determined for C1–3, S1 and S2 samples. Weight % of magnetite (M) in the samples measured in this study is indicated in brackets.

The C1, C2 and C3 ore samples (Fig. 1A) showed high concentrations of Al and Mg (>2000 mg kg^{-1}), V (685–11,188 mg kg^{-1}), Mn (147–2060 mg kg^{-1}), Ni (69–522 mg kg^{-1}), Zn (48–132 mg kg^{-1}) and Co (28–186 mg kg^{-1}). Variable amounts were observed for Ti (16–2114 mg kg^{-1}), Cu (2–407 mg kg^{-1}), Cr (2–363 mg kg^{-1}) and Ga (2–126 mg kg^{-1}), and a relatively low one for Pb (<2 mg kg^{-1}). The highest values of Cu and Cr in magnetite were observed for the C3 sample, which also contained chalcopyrite. In general, the Swedish S1 and S2 ore samples (Fig. 1B) exhibited a TEs composition pattern of magnetite relatively similar to that observed for the C1 and C2 samples from the Chilean Iron Oxide Apatite (IOA) deposits (Fig. 1A). Nevertheless, the S2 sample showed lower concentrations of Zn, Cu, Pb and Y. In addition to the elements shown in Fig. 1, As was also detected and showed average values of up to ≈230 mg kg^{-1} in S2 and C5-T. Further comparison between TEs composition in magnetite from different deposits in Chile and Sweden and literature data is shown in SM (Fig. S2).

The elemental composition of the magnetite in the processed ore tailings sample (CT) is illustrated in Fig. 1C. The As concentration range determined by LA-ICP-MS and EMPA was 143–213 mg kg^{-1}. Reported TEs concentrations in magnetite ore samples from this deposit (LC-04\05 and LC-14, Knipping et al. (2015), Fig. 1C) generally fall within the range of those of the magnetite ore samples of the present study (shaded area, Fig. 1). Except for Cr and Ti, the average TEs concentrations of the magnetite grains in the CT sample were higher than those in the LC-04\05 and LC-14 samples. Likewise, the average concentrations of several elements in the CT sample (e.g., Co, Mg and Al) were much higher than the range obtained for the magnetite ore samples measured in the present study (shaded area in Fig. 1).

In order to investigate further the TEs concentrations in the magnetite from the tailings, EMPA analyses were carried out on the CT sample and a magnetite ore sample from the mine (C5-T) (Fig. S3 in SM). The elemental composition of the C5-T sample determined by total acid digestion agreed well with the literature bulk rock measurements (Knipping et al., 2015). EMPA results showed that i) the concentration of most of the elements was higher in the magnetite of the tailings (CT) than that in the magnetite ore sample (C5-T), and ii) the differences in the TEs concentrations of magnetite between samples CT and C5-T (Fig. S3 in SM) are in general smaller than those observed between CT and LC-04\05 and LC-14 by LA-ICP-MS (Fig. 1C). Therefore, LA-ICP-MS and EMPA results indicate elevated contents of TEs in the magnetite of the tailings (Fig. 1C and Fig. S3 in SM), which are even higher than in the magnetite ore samples from the same ore deposit (i.e., non-processed material). A hypothesis for the high content of TEs in the tailings' magnetite is a TEs enrichment during the iron separation process in the iron concentration plant (see Sections 5 and 6 in SM). This accurate determination of the TEs concentrations is relevant to evaluate the potential impact of TEs release on marine environments affected by STD.

3.2. Magnetite bioreduction

In all biotic experiments, the measured concentrations of dissolved iron (Fig. 2 and Fig. S5 in SM) were much higher than those in the abiotic controls (either prepared under atmospheric or anoxic conditions). The acetate formation coupled to lactate consumption observed in the biotic experiments indicated ferric iron bioreduction as expressed in Eq. (2). Iron speciation measurements indicated that the iron in solution was Fe(II), which agrees with the pH (8.0 ± 0.1, ±1σ), Eh_{std} (45 ± 24 mV, ±1σ) and DO (<0.05 mg L^{-1}) values observed during the experiments with the magnetite-bearing samples and the PHREEQC speciation calculations.

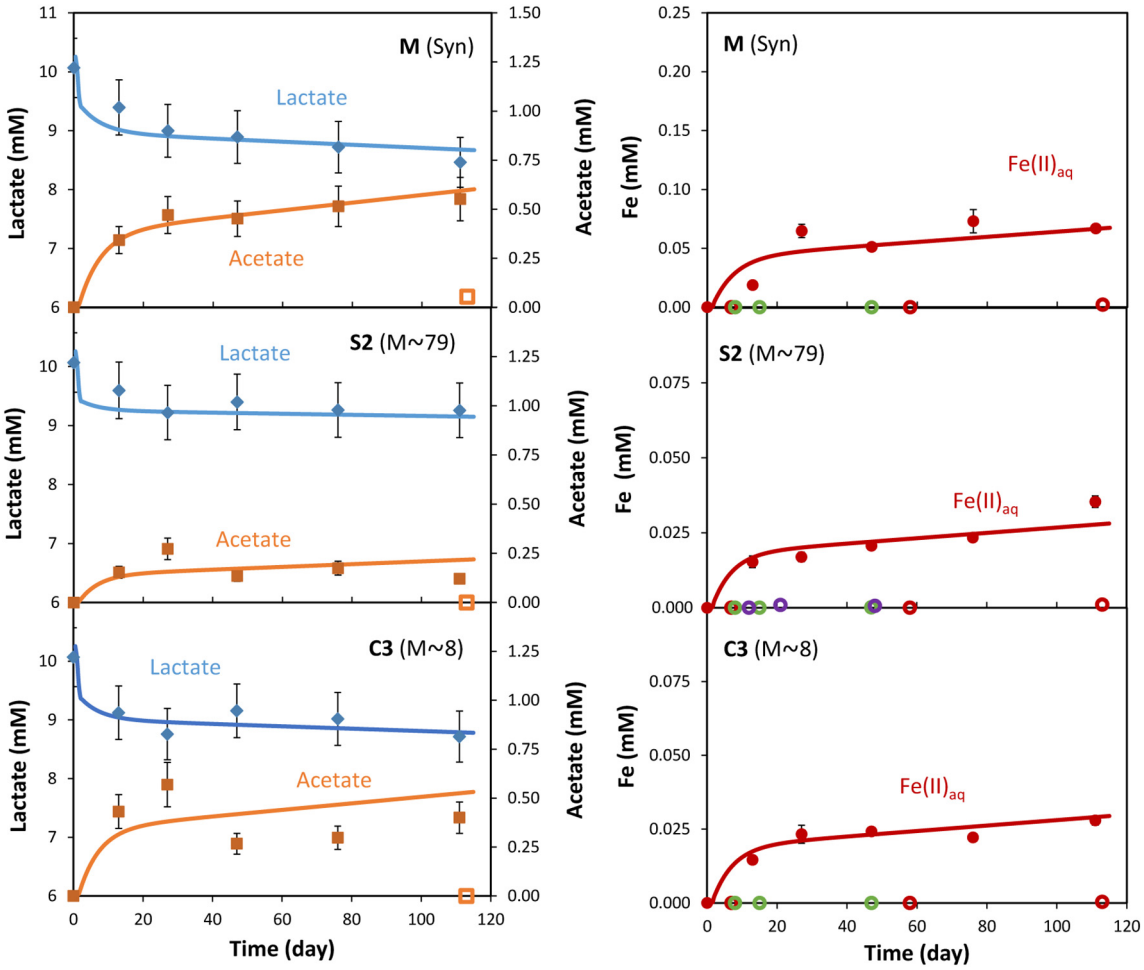

Fig. 2. Evolution of lactate, acetate and dissolved Fe(II) during the experiments. Solid lines represent the trends obtained by model simulations. Representative experiments with synthetic magnetite (M (Syn)) and ore samples from different locations (Chile (C3) and Sweden (S2)) and with different amounts of magnetite were selected. Weight % of magnetite (M) in the samples is indicated in brackets. Concentrations of acetate (empty squares, left panels) and $Fe(II)_{aq}$ (red empty circles, right panels) in the abiotic controls are indicated. Also, $Fe(II)_{aq}$ concentrations from the anoxic abiotic controls prepared using O_2-free water, either ASW (violet) or Milli-Q water (green), are shown. Abiotic controls prepared using O_2-free ASW were only performed for some samples. Concentration data plots for the other magnetite-bearing samples and synthetic iron minerals are available in the SM (Fig. S5).

As the bioreduction experiments were prepared under oxic conditions, iron reduction started after oxygen consumption. Previous tests prepared and conducted similarly, using either ferric-citrate or ferrihydrite as the source of Fe(III), showed initial oxic conditions for approximately 2 days. Thus, lactate was initially consumed by aerobic oxidation to CO_2 and microbial growth (Eq. (S1) in SM). The aerobic metabolic pathway was also included in the geochemical model and Y values used in Eq. (3) for oxic and anoxic conditions are indicated in the SM (Table S4). In fact, a transition from (sub)oxic to anoxic (iron reducing) conditions is likely to occur in seabed sediments impacted by STD. Strong redox gradients are common in the sediment-water interface (Devol, 2015; Santschi et al., 1990), and typical DO penetration depths in fine sediments in highly productive coastal waters are no more than 1 cm (Morello et al., 2016). In the experiments with ferryhidrite, initial lactate concentration (10 mM) was totally consumed after 20 days (Fig. S5-F in SM). By contrast, the estimated total lactate consumption (as electron donor and carbon source) for the experiments with magnetite ranged between 8.1 and 13.3% (Fig. 2 and Table S5 in SM). Similar values were obtained for the experiments with hematite and goethite (Table S5 in SM).

The maximum substrate consumption rates (k_{max}, Eq. (1)) under oxic (4.4×10^{-5} s^{-1} for all experiments) and anoxic conditions (from 6.6×10^{-7} to 2.5×10^{-6} s^{-1} for experiments with magnetite; Table S4 in SM) were derived by model calibration, based on both the lactate consumption and acetate formation during the experiments. Similar values were determined for the experiments with hematite and goethite, with the exception of the higher value obtained for ferrihydrite (2.3×10^{-5} s^{-1}), which is consistent with the much higher specific surface area of this sample (Table S1 in SM). For the experiments with magnetite samples, the highest k_{max} value was obtained for the experiments with synthetic magnetite (2.5×10^{-6} s^{-1}), which also had a specific surface area higher than those of the magnetite ore samples (Table S1 in SM). Nevertheless, the magnetite experiments showed a relatively narrow range of $k_{m_{ox}}$ values (average value of $1.3 \times 10^{-6} \pm 0.7 \times 10^{-6}$ s^{-1}, $\pm 1\sigma$, $n = 8$; Table S4 in SM).

Simulations reproduced satisfactorily the trends of experimental lactate consumption and acetate formation (Fig. 2 and Fig. S5 in SM). Under the conditions investigated, the consumption of lactate was higher in oxic conditions, except for the ferrihydrite experiments, in which lactate was mainly consumed via oxidation to acetate under anoxic conditions (Fig. S5-F in SM). Under anoxic conditions, concentrations of acetate and dissolved Fe(II) showed a similar evolution for most of the experiments regardless of the solid sample used (Fig. 2 and Fig. S5 in SM). Concentrations of acetate and dissolved Fe(II) exhibited a relatively rapid increase for approximately 10 days. Thereafter, the rate of the increase was much lower or close to zero (e.g., Fig. S5-CT in SM).

With the model parameters (Table S4 in SM), the numerical simulations indicate an increase in cell biomass (i.e., X in Eqs. (1) and (3)) under oxic conditions, followed by a reduction of biomass when solid Fe^{3+} is used as electron acceptor (see Section 11 in SM). An exception is ferrihydrite, where microbial growth might be also possible under iron reducing conditions. Compared to the other Fe^{3+}-bearing minerals used in the experiments, Fe^{3+} in ferrihydrite is more bioavailable due to the low crystallinity and high surface area of this phase (Table S1 in SM). Therefore, under the investigated conditions, a reduction of cell biomass may explain the attenuation of iron reduction in the experiments. Such reduction of cell biomass might be interpreted either as a decrease in the number of active cells or as a constant number of cells with slower metabolism. It reflects the lower bioavailability of solid Fe^{3+} in iron (hydr)oxides compared to dissolved electron acceptors (e.g., oxygen or ferric-citrate), and also the potential occurrence of processes inhibiting Fe(III) bioreduction. For instance, previous studies investigated the inhibitory effect of Fe(II) on bacterial activity (Burgos et al., 2002; Liu et al., 2001b; Urrutia et al., 1998).

3.3. Release of Fe(II) and TEs

On the basis of lactate consumption and acetate formation in the experiments with magnetite-bearing samples, estimations of total ferric iron reduction (relative to the initial content of Fe^{3+} in the solid samples, Table S5 in SM) ranged between 1.3% and 3.7% for the samples with high amounts of ferric iron (from 31.8 to 88.4 mM Fe^{3+}) and between 33.2% and 90.1% for the samples with low amounts (from 1.9 to 7.7 mM Fe^{3+}). The highest relative amount of ferric iron reduction (up to 90.1%) corresponds to the iron ore tailings, which could explain the iron reduction cessation after 20 days (Fig. S5-CT in SM). For the experiments with synthetic hematite and goethite samples, slightly lower values (1.1 and 1.4%, respectively) were determined compared to synthetic magnetite (3.7%), whereas the iron reduction was higher for ferrihydrite (35.4%).

According to the estimated total Fe(III) bioreduction in the experiments, the expected concentrations of Fe(II) in solution were much higher than those measured, suggesting that dissolved Fe(II) only represented a minor fraction of the total ferric iron reduced. Previous studies showed that aqueous Fe(II) reacts on the surface of iron oxide minerals such as hematite, goethite, ferrihydrite and magnetite (Gorski and Scherer (2011) and references therein). In accordance with these studies, adsorbed Fe(II) on magnetite oxidizes to Fe(III) by electron transfer to the mineral phase, resulting in magnetite growth (Eq. (S2) in SM). The examination of the solid samples retrieved at the end of the experiments (Figs. S6 and S7 in SM) supports the formation of magnetite as the main biogenic Fe^{2+}-bearing mineral during Fe(III) bioreduction under the investigated conditions.

Detailed experiments in previous studies revealed that the uptake of Fe(II) from the aqueous phase is controlled by the ratio of Fe^{2+}/Fe^{3+} in magnetite (e.g., for stoichiometric magnetite ($Fe^{2+}Fe^{3+}_2O_4$) the Fe^{2+}/Fe^{3+} ratio is 0.5), being higher in experiments with partially oxidized magnetite (i.e., Fe^{3+}-enriched, $Fe^{2+}/Fe^{3+} < 0.5$) (Gorski and Scherer, 2009). This process was considered in the geochemical model for the experiments with magnetite-bearing samples (see SM, Section 8). The Fe^{2+}/Fe^{3+} ratios of magnetite for different samples (from 0.20 to 0.35, Table S5 in SM) were determined by model calibration based on the measured aqueous Fe(II). These ratios are similar to those available in the literature i) for natural magnetite samples (e.g., $0.23 < Fe^{2+}/Fe^{3+} < 0.34$, Gorski and Scherer (2009)) and ii) after exposing stoichiometric synthetic magnetite to ambient air for 24 h ($Fe^{2+}/Fe^{3+} = 0.24$, Cheng et al. (2018)). Note that during reductive dissolution of partially oxidized magnetite a lesser amount of structural Fe^{2+} per mole of magnetite dissolved is released to the solution compared to stoichiometric magnetite.

Simulations indicated that the uptake of dissolved Fe(II) by oxidation on magnetite could explain the aqueous Fe(II) concentrations measured in the experiments with samples containing relatively high amounts of magnetite (i.e., >30 wt%). In samples with lower fractions of magnetite (i.e., <10 wt%), oxidation of dissolved Fe(II) and magnetite growth explains partially the measured aqueous Fe(II) concentrations (even considering in the simulations oxidized magnetite with a Fe^{2+}/Fe^{3+} of 0.2), suggesting a potential precipitation of other secondary Fe^{2+}-bearing minerals such as siderite ($Fe^{2+}CO_3$). Secondary siderite precipitation was observed in previous studies of Fe(III) bioreduction of magnetite (Dong et al., 2000), goethite (Liu et al., 2001a) and ferric-citrate (Castro et al., 2018) at circumneutral pH. Thus, siderite precipitation was contemplated in the geochemical modeling (Eq. (S3) and Tables S3 and S5 in SM) of the experiments with samples containing low amounts of magnetite (<10 wt%). The saturation index with respect to siderite calculated by PHREEQC at the end of all the experiments with magnetite-containing samples ranged between −0.42 and 0.41 (Table S5 in SM), indicating near-equilibrium conditions. Hence, experimental and model results suggest that the amount of magnetite in sediments impacted by STD might be an important factor controlling the formation of different secondary Fe^{2+}-bearing minerals (e.g., magnetite and/or siderite). This could have strong implications on the distribution of trace metals eventually released during iron (hydr)oxides reductive dissolution in the environment.

The maximum rates of aqueous Fe(II) concentration increase (Fig. 2 and Fig. S5 in SM) were estimated based on the simulations. Values from 0.07 to 0.26 μM h^{-1} were determined for the experiments with magnetite containing samples. The rates for the experiments with synthetic hematite and goethite were within the range of magnetite containing samples, whereas the rate determined for ferrihydrite (4.4 μM h^{-1}) was clearly above.

Along with Fe, several trace metal(loid)s (Mn, V, As and Cu) were detected in solution (<1 mg L^{-1}) (Fig. 3). According to inorganic speciation calculations, elements released in solution under the investigated conditions mainly existed as free species and chloride complexes (i.e., Fe^{2+}, Mn^{2+}, $FeCl^+$, $MnCl^+$, $CuCl_3^{2-}$, $CuCl^-$). Arsenic was mainly found as As(III) (i.e., H_3AsO_3), which is more toxic than As(V) (Jain and Ali, 2000). It might increase the concentrations of labile TEs in sediments impacted by STD. Mn and V were among those TEs with high concentrations in the magnetite ore samples (Fig. 1). Other elements (Ni and Ga) were detected in solution only in few samples and/or at lower concentrations (Fig. 3). However, Ni concentrations in the magnetite ore samples were in general relatively high, similar to those of Mn (Fig. 1). Similarly, despite Co and Ti concentrations were above 100 mg Kg^{-1} in some magnetite samples, they were never detected in solution (detection limits of 2 and 7 μg·L^{-1}, respectively). These results suggest that other processes, including coprecipitation within secondary biogenic Fe^{2+}-minerals, may control the fate of elements such as Ni, Co and Ti during reductive dissolution of magnetite under the investigated conditions, which is in agreement with the

	Fe	Mn	V	As	Cu	Ni	Ga
S1 (M~35)	2367	65					
S2 (M~79)	1974	35				12	
C1 (M~89)	880	42			328		
C2 (M < 5)	2394	126					
C3 (M~8)	1560	116			148		
C4 (M~19/H~40)	3386	134	79	17			
C5-T (M~90)	2447	137	15	12		72	
CT (M < 5)	729	203	24	14			21

Fig. 3. Elements detected in solution during the iron bioreduction experiments with different magnetite ore samples and the tailings sample. *Dark orange*: elements detected in all the tubes. *Orange*: elements detected in all the tubes at lower concentrations. *Pale orange*: elements detected at very low concentrations or in part of the tubes. The highest concentrations (μg L^{-1}) determined for each solid used in the experiments (n = 5) are indicated.

observations of previous Fe(III) bioreduction studies using synthetic oxyhydroxides coprecipitated with either Co or Ni (Coker et al., 2008; Zachara et al., 2001). For instance, Coker et al. (2008) determined the incorporation and site occupancies of Co and Ni into the structure of biogenic magnetite (see additional information in SM).

To investigate further the fate of TEs in more detail, a stoichiometric release of TEs to the aqueous phase during magnetite reductive dissolution was simulated for two magnetite ore samples (C1 and C5-T) and the tailings sample (CT) (Fig. 4). The stoichiometric coefficients for the different elements were estimated by model calibration according to their aqueous concentrations, and the resulting values were compared with those expected according to the TEs composition of magnetite in the respective samples (see SM). The results suggest that part of As and V released by reductive dissolution of magnetite in C5-T and CT samples might be incorporated to secondary biogenic minerals (mainly magnetite) and/or adsorbed on the remaining magnetite and gangue minerals. Guo et al. (2007) showed removal of As(III) and As(V) from solution at neutral pH (higher from As(III)- than from As(V)-solution) associated with coprecipitation of Fe(III) oxides and subsequently adsorption of As on the fresh Fe(III) oxides. Wang et al. (2008) investigated the interaction of aqueous As(III) during magnetite precipitation experiments at neutral pH and observed arsenite sequestration via surface adsorption and surface precipitation reactions. In the present study, As in solution was mainly H_3AsO_3 suggesting that the effect of adsorption might be limited by the lack of electrostatic attraction compared with other aqueous As species.

4. Conclusions

Magnetite showed elevated contents of TEs, which are higher in the magnetite of the tailings than in those of the ore samples from different mines. The experimental data indicated that iron oxides such as magnetite can undergo reductive dissolution under marine sediment conditions, leading to a release of Fe and associated TEs (e.g., Mn, V, As and Cu) to the aqueous phase. Therefore, this process can increase the concentrations of labile TEs in pore water of marine sediments impacted by STD. Model results suggest that the concentration of magnetite in the sediments and its Fe^{2+}/Fe^{3+} ratio are important factors controlling the fate and mobility of Fe(II) and TEs.

In addition to the potential adverse impacts of TEs on the marine fauna, solubilization of Fe, a limiting nutrient for phytoplankton production (Boyd et al., 2000), could lead to fertilization and subsequent eutrophication processes, which may result in oxygen depletion and expansion of the oxygen minimum zone (Breitburg et al., 2018). Thus, besides the known smothering of benthic organisms and physical alteration of seabed habitats in areas affected by STD, reductive dissolution of iron (hydr)oxide minerals and subsequent release of Fe and TEs have to be considered as potential negative impacts on the marine ecosystem.

Author contributions

The manuscript was written through contributions of all authors. All authors have given approval to the final version of the manuscript.

CRediT authorship contribution statement

Jordi Palau: Conceptualization, Methodology, Investigation, Formal analysis, Writing – original draft, Writing – review & editing. **Robert Benaiges-Fernandez:** Conceptualization, Methodology, Investigation, Writing – review & editing. **Francesco Offeddu:** Methodology, Investigation, Writing – review & editing. **Jordi Urmeneta:** Conceptualization, Methodology, Supervision. **Josep M. Soler:** Methodology, Formal analysis, Writing – review & editing. **Jordi Cama:** Conceptualization, Methodology, Validation, Writing – review & editing, Supervision, Project administration. **Bernhard Dold:** Conceptualization, Methodology, Validation, Writing – review & editing, Supervision, Project administration, Funding acquisition.

Declaration of competing interest

The authors declare that they have no known competing financial interests or personal relationships that could have appeared to influence the work reported in this paper.

Acknowledgements

Thanks are due to Jordi Bellés (IDAEA-CSIC) for technical assistance in the laboratory and to Prof. Carlos Ayora (IDAEA-CSIC) for the fruitful discussions on the geochemical model implementation. Technical and human support provided by the Geochronology and Isotope Geochemistry-SGIker facility (UPV/EHU, MINECO, GV/EJ, ERDF and ESF) is gratefully acknowledged. This study was funded by the Chilean Government through the Research Fund for Fishery and Aquaculture (Fondo de Investigación Pesquera y de Acuicultura; FIPA) of SUBPESCA (FIP 2015-11 project), the Spanish Ministries of Economy and Competitiveness and Science and Innovation with contribution of FEDER funds (CGL2017–82331-R and CEX2018-000794-S projects), and the Catalan Government (2017SGR 1733 project). We thank the three anonymous reviewers whose comments and suggestions contributed to improve the quality of the manuscript.

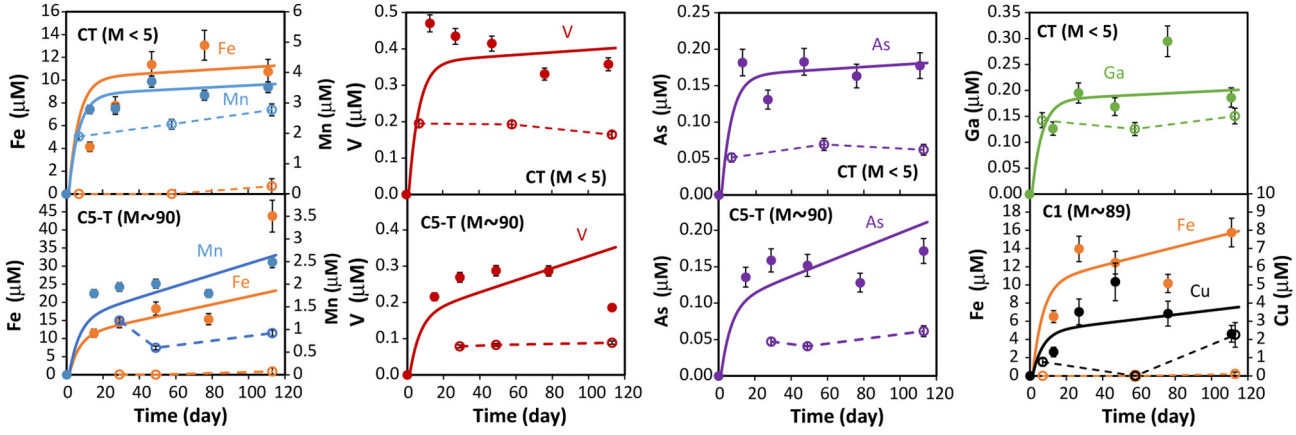

Fig. 4. Evolution of dissolved Fe(II) and selected TEs during the experiments. Solid lines represent the trends obtained by numerical simulations. Empty symbols and dashed lines correspond to the concentrations determined in the abiotic controls. Weight % of magnetite (M) in the samples is indicated in brackets.

Appendix A. Supplementary material

Further information about experiment set up details, analytical methods, geochemical model settings and additional figures is available. Supplementary material to this article can be found online at https://doi.org/10.1016/j.scitotenv.2021.147579.

References

Angel, B.M., Simpson, S.L., Jarolimek, C.V., Jung, R., Waworuntu, J., Batterham, G., 2013. Trace metals associated with deep-sea tailings placement at the Batu Hijau copper-gold mine, Sumbawa, Indonesia. Mar. Pollut. Bull. 73, 306–313. https://doi.org/10.1016/j.marpolbul.2013.04.013.

Bish, D.L., Howard, S.A., 1988. Quantitative phase-analysis using the Rietveld method. J. Appl. Crystallogr. 21, 86–91. https://doi.org/10.1107/s0021889887009415.

Boutroy, E., Dare, S.A.S., Beaudoin, G., Barnes, S.-J., Lightfoot, P.C., 2014. Magnetite composition in Ni-Cu-PGE deposits worldwide: application to mineral exploration. J. Geochem. Explor. 145, 64–81. https://doi.org/10.1016/j.gexplo.2014.05.010.

Boyd, P.W., Watson, A.J., Law, C.S., Abraham, E.R., Trull, T., Murdoch, R., Bakker, D.C., Bowie, A.R., Buesseler, K.O., Chang, H., Charette, M., Croot, P., Downing, K., Frew, R., Gall, M., Hadfield, M., Hall, J., Harvey, M., Jameson, G., LaRoche, J., Liddicoat, M., Ling, R., Maldonado, M.T., McKay, R.M., Nodder, S., Pickmere, S., Pridmore, R., Rintoul, S., Safi, K., Sutton, P., Strzepek, R., Tanneberger, K., Turner, S., Waite, A., Zeldis, J., 2000. A mesoscale phytoplankton bloom in the polar Southern Ocean stimulated by iron fertilization. Nature 407, 695–702. https://doi.org/10.1038/35037500.

Breitburg, D., Levin, L.A., Oschlies, A., Gregoire, M., Chavez, F.P., Conley, D.J., Garcon, V., Gilbert, D., Gutierrez, D., Isensee, K., Jacinto, G.S., Limburg, K.E., Montes, I., Naqvi, S.W.A., Pitcher, G.C., Rabalais, N.N., Roman, M.R., Rose, K.A., Seibel, B.A., Telszewski, M., Yasuhara, M., Zhang, J., 2018. Declining oxygen in the global ocean and coastal waters. Science (80-.), 359 https://doi.org/10.1126/science.aam7240.

Brunauer, S., Emmett, P.H., Teller, E., 1938. Adsorption of gases in multimolecular layers. J. Am. Chem. Soc. 60, 309–319. https://doi.org/10.1021/ja01269a023.

Buch, A.C., Niemeyer, J.C., Marques, E.D., Silva-Filho, E.V., 2021. Ecological risk assessment of trace metals in soils affected by mine tailings. J. Hazard. Mater. https://doi.org/10.1016/j.jhazmat.2020.123852.

Burgos, W.D., Royer, R.A., Fang, Y.L., Yeh, G.T., Fisher, A.S., Jeon, B.H., Dempsey, B.A., 2002. Theoretical and experimental considerations related to reaction-based modeling: a case study using iron(III) oxide bioreduction. Geomicrobiol J. 19, 253–287. https://doi.org/10.1080/01490450252864299.

Castro, L., Luisa Blazquez, M., Gonzalez, F., Munoz, J.A., Ballester, A., 2018. Heavy metal adsorption using biogenic iron compounds. Hydrometallurgy 179, 44–51. https://doi.org/10.1016/j.hydromet.2018.05.029.

Cheng, W., Marsac, R., Hanna, K., 2018. Influence of magnetite stoichiometry on the binding of emerging organic contaminants. Environ. Sci. Technol. 52, 467–473. https://doi.org/10.1021/acs.est.7b04849.

Coker, V.S., Pearce, C.I., Pattrick, R.A.D., van der Laan, G., Telling, N.D., Charnock, J.M., Arenholz, E., Lloyd, J.R., 2008. Probing the site occupancies of Co-, Ni-, and Mn-substituted biogenic magnetite using XAS and XMCD. Am. Mineral. 93, 1119–1132. https://doi.org/10.2138/am.2008.2681.

Dare, S.A.S., Barnes, S.-J., Beaudoin, G., Meric, J., Boutroy, E., Potvin-Doucet, C., 2014. Trace elements in magnetite as petrogenetic indicators. Mineral. Deposita 49, 785–796. https://doi.org/10.1007/s00126-014-0529-0.

Devol, A.H., 2015. Denitrification, anammox, and N(2) production in marine sediments. Annu. Rev. Mar. Sci. 7, 403–423. https://doi.org/10.1146/annurev-marine-010213-135040.

Dold, B., 2014a. Evolution of acid mine drainage formation in sulphidic mine tailings. Minerals 4, 621–641. https://doi.org/10.3390/min4030621.

Dold, B., 2014b. Submarine tailings disposal (STD)-a review. Minerals 4, 642–666. https://doi.org/10.3390/min4030642.

Dold, B., Gonzalez-Toril, E., Aguilera, A., Lopez-Pamo, E., Cisternas, M.E., Bucchi, F., Amils, R., 2013. Acid rock drainage and rock weathering in Antarctica: important sources for iron cycling in the Southern Ocean. Environ. Sci. Technol. 47, 6129–6136. https://doi.org/10.1021/es305141b.

Dong, H., Fredrickson, J.K., Kennedy, D.W., Zachara, J.M., Kukkadapu, R.K., Onstott, T.C., 2000. Mineral transformations associated with the microbial reduction of magnetite. Chem. Geol. 169, 299–318. https://doi.org/10.1016/S0009-2541(00)00210-2.

Embile Jr., R.F., Walder, I.F., Schuh, C., Donatelli, J.L., 2018. Cu, Pb and Fe release from sulfide-containing tailings in seawater: results from laboratory simulation of submarine tailings disposal. Mar. Pollut. Bull. 137, 582–592. https://doi.org/10.1016/j.marpolbul.2018.11.012.

Gambi, C., Canals, M., Corinaldesi, C., Dell'Anno, A., Manea, E., Pusceddu, A., Sanchez-Vidal, A., Danovaro, R., 2020. Impact of historical sulfide mine tailings discharge on meiofaunal assemblages (Portman Bay, Mediterranean Sea). Sci. Total Environ. 736. https://doi.org/10.1016/j.scitotenv.2020.139641.

Gao, H., Obraztova, A., Stewart, N., Popa, R., Fredrickson, J.K., Tiedje, J.M., Nealson, K.H., Zhou, J., 2006. Shewanella loihica sp. nov., isolated from iron-rich microbial mats in the Pacific Ocean. Int. J. Syst. Evol. Microbiol. 56, 1911–1916. https://doi.org/10.1099/ijs.0.64354-0.

Geng, H., Wang, F., Yan, C., Tian, Z., Chen, H., Zhou, B., Yuan, R., Yao, J., 2020. Leaching behavior of metals from iron tailings under varying pH and low-molecular-weight organic acids. J. Hazard. Mater. https://doi.org/10.1016/j.jhazmat.2019.121136.

Gorski, C.A., Scherer, M.M., 2009. Influence of magnetite stoichiometry on Fe-II uptake and nitrobenzene reduction. Environ. Sci. Technol. 43, 3675–3680. https://doi.org/10.1021/es803613a.

Gorski, C.A., Scherer, M.M., 2011. Fe2+ sorption at the Fe oxide-water Interface: a revised conceptual framework. In: Tratnyek, P.G., Grundl, T.J., Haderlein, S.B. (Eds.), Aquatic Redox Chemistry, ACS Symposium Series, pp. 315–343.

Guo, H., Stüben, D., Berner, Z., 2007. Adsorption of arsenic(III) and arsenic(V) from groundwater using natural siderite as the adsorbent. J. Colloid Interface Sci. 315, 47–53. https://doi.org/10.1016/j.jcis.2007.06.035.

Hughes, D.J., Shimmield, T.M., Black, K.D., Howe, J.A., 2015. Ecological impacts of large-scale disposal of mining waste in the deep sea. Sci. Rep. 5, 11. https://doi.org/10.1038/srep09985.

Jain, C.K., Ali, I., 2000. Arsenic: occurrence, toxicity and speciation techniques. Water Res. 34, 4304–4312. https://doi.org/10.1016/S0043-1354(00)00182-2.

Kappler, A., Straub, K.L., 2005. Geomicrobiological cycling of iron. In: Banfield, J.E., CerviniSilva, J., Nealson, K.H. (Eds.), Molecular Geomicrobiology, Reviews in Mineralogy & Geochemistry, pp. 85–108 https://doi.org/10.2138/rmg.2005.59.5.

Knipping, J.L., Bilenker, L.D., Simon, A.C., Reich, M., Barra, F., Deditius, A.P., Waelle, M., Heinrich, C.A., Holtz, F., Munizaga, R., 2015. Trace elements in magnetite from massive iron oxide-apatite deposits indicate a combined formation by igneous and magmatic-hydrothermal processes. Geochim. Cosmochim. Acta 171, 15–38. https://doi.org/10.1016/j.gca.2015.08.010.

Koski, R.A., 2012. Metal dispersion resulting from mining activities in coastal environments: a pathways approach. Oceanography 25, 170–183. https://doi.org/10.5670/oceanog.2012.53.

Liu, C., Kota, S., Zachara, J.M., Fredrickson, J.K., Brinkman, C.K., 2001a. Kinetic analysis of the bacterial reduction of goethite. Environ. Sci. Technol. 35, 2482–2490. https://doi.org/10.1021/es001956c.

Liu, C., Zachara, J.M., Gorby, Y.A., Szecsody, J.E., Brown, C.F., 2001b. Microbial reduction of Fe(III) and sorption/precipitation of Fe(II) on Shewanella putrefaciens strain CN32. Environ. Sci. Technol. 35, 1385–1393. https://doi.org/10.1021/es0015139.

Lottermoser, B.G., 2010. Mine Wastes: Characterization, Treatment and Environmental Impacts, Mine Wastes: Characterization, Treatment and Environmental Impacts. Springer-Verlag, Berlin, Berlin https://doi.org/10.1007/978-3-642-12419-8.

Lovley, D.R., Holmes, D.E., Nevin, K.P., 2004. Dissimilatory Fe(III) and Mn(IV) reduction. In: Poole, R.K. (Ed.), Advances in Microbial Physiology. Advances in Microbial Physiology vol. 49, pp. 219–286. https://doi.org/10.1016/s0065-2911(04)49005-5.

Maier, R.M., 2009. Chapter 3 - bacterial growth. In: Maier, R.M., Pepper, I.L., Gerba, C.P. (Eds.), Environmental Microbiology, Second edition Academic Press, San Diego, pp. 37–54 https://doi.org/10.1016/B978-0-12-370519-8.00003-1.

Makvandi, S., Ghasemzadeh-Barvarz, M., Beaudoin, G., Grunsky, E.C., McClenaghan, M.B., Duchesne, C., 2016. Principal component analysis of magnetite composition from volcanogenic massive sulfide deposits: case studies from the Izok Lake (Nunavut, Canada) and Halfmile Lake (New Brunswick, Canada) deposits. Ore Geol. Rev. 72, 60–85. https://doi.org/10.1016/j.oregeorev.2015.06.023.

Manteca, J.I., López García, J.Á., Oyarzun, R., Carmona, C., 2014. The beach placer iron deposit of Portman Bay, Murcia, SE Spain: the result of 33 years of tailings disposal (1957-1990) to the Mediterranean seaside. Mineral. Deposita 49, 777–783. https://doi.org/10.1007/s00126-014-0511-x.

Morello, E.B., Haywood, M.D.E., Brewer, D.T., Apte, S.C., Asmund, G., Kwong, Y.T.J., Dennis, D., 2016. The ecological impacts of submarine tailings placement. In: Hughes, R.N., Hughes, D.J., Smith, I.P., Dale, A.C. (Eds.), Oceanography and Marine Biology: An Annual Review. Oceanography and Marine Biology vol. 54, pp. 315–366 (Crc Press-Taylor & Francis Group, [Morello, Elisabetta B.; Haywood, Michael D. E.; Brewer, David T.; Dennis, Darren] CSIRO Oceans & Atmosphere, Ecosci Precinct, 41 Boggo Rd, Dutton Pk, Qld 4102, Australia. [Morello, Elisabetta B.] CNR Natl Res Council Italy, ISMAR Marine Sci Inst, Largo F).

Nadoll, P., Angerer, T., Mauk, J.L., French, D., Walshe, J., 2014. The chemistry of hydrothermal magnetite: a review. Ore Geol. Rev. 61, 1–32. https://doi.org/10.1016/j.oregeorev.2013.12.013.

Nadoll, P., Mauk, J.L., Leveille, R.A., Koenig, A.E., 2015. Geochemistry of magnetite from porphyry Cu and skarn deposits in the southwestern United States. Mineral. Deposita 50, 493–515. https://doi.org/10.1007/s00126-014-0539-y.

Nystrom, J.O., Henriquez, F., 1994. Magmatic features of iron-ores of the Kiruna type in Chile and Sweden - ore textures and magnetite geochemistry. Econ. Geol. 89, 820–839. https://doi.org/10.2113/gsecongeo.89.4.820.

Parkhurst, D.L., Appelo, C.A.J., 1999. User's Guide to PHREEQC (Version 2)—A Computer Program for Speciation, Reaction-Path, Advective-Transport, and Inverse Geochemical Calculations. USGS Water-Resources Investigation.

Pedersen, K.B., Jensen, P.E., Sternal, B., Ottosen, L.M., Henning, M.V., Kudahl, M.M., Junttila, J., Skirbekk, K., Frantzen, M., 2018. Long-term dispersion and availability of metals from submarine mine tailing disposal in a fjord in Arctic Norway. Environ. Sci. Pollut. Res. Int. 25, 32901–32912. https://doi.org/10.1007/s11356-017-9276-y.

Ramirez-Llodra, E., Trannum, H.C., Evenset, A., Levin, L.A., Andersson, M., Finne, T.E., Hilario, A., Flem, B., Christensen, G., Schaanning, M., Vanreusel, A., 2015. Submarine and deep-sea mine tailing placements: a review of current practices, environmental issues, natural analogs and knowledge gaps in Norway and internationally. Mar. Pollut. Bull. 97, 13–35. https://doi.org/10.1016/j.marpolbul.2015.05.062.

Ribet, I., Ptacek, C.J., Blowes, D.W., Jambor, J.L., 1995. The potential for metal release by reductive dissolution of weathered mine tailings. J. Contam. Hydrol. 17, 239–273. https://doi.org/10.1016/0169-7722(94)00010-F.

Rico, M., Benito, G., Diez-Herrero, A., 2008. Floods from tailings dam failures. J. Hazard. Mater. 154, 79–87. https://doi.org/10.1016/j.jhazmat.2007.09.110.

Roden, E.E., Jin, Q., 2011. Thermodynamics of microbial growth coupled to metabolism of glucose, ethanol, short-chain organic acids, and hydrogen. Appl. Environ. Microbiol. 77, 1907–1909. https://doi.org/10.1128/AEM.02425-10.

Roh, Y., Gao, H., Vali, H., Kennedy, D.W., Yang, Z.K., Gao, W., Dohnalkova, A.C., Stapleton, R.D., Moon, J.W., Phelps, T.J., Fredrickson, J.K., Zhou, J., 2006. Metal reduction and iron biomineralization by a psychrotolerant Fe(III)-reducing bacterium, Shewanella

sp. strain PV-4. Appl. Environ. Microbiol. 72, 3236–3244. https://doi.org/10.1128/AEM.72.5.3236-3244.2006.
Santschi, P., Hohener, P., Benoit, G., Buchholtztenbrink, M., 1990. Chemical processes at the sediment water interface. Mar. Chem. 30, 269–315. https://doi.org/10.1016/0304-4203(90)90076-o.
Schwertmann, U., Cornell, R.M., 2000. Iron Oxides in the Laboratory: Preparation and Characterization. Second. ed. WILEY-VCH Verlag GmbH https://doi.org/10.1002/9783527613229.
Simpson, S.L., Spadaro, D.A., 2016. Bioavailability and chronic toxicity of metal sulfide minerals to benthic marine invertebrates: implications for Deep Sea exploration, mining and tailings disposal. Environ. Sci. Technol. 50, 4061–4070. https://doi.org/10.1021/acs.est.6b00203.
Sternal, B., Junttila, J., Skirbekk, K., Forwick, M., Carroll, J., Pedersen, K.B., 2017. The impact of submarine copper mine tailing disposal from the 1970s on Repparfjorden, northern Norway. Mar. Pollut. Bull. 120, 136–153. https://doi.org/10.1016/j.marpolbul.2017.04.054.
Thullner, M., Van Cappellen, P., Regnier, P., 2005. Modeling the impact of microbial activity on redox dynamics in porous media. Geochim. Cosmochim. Acta 69, 5005–5019. https://doi.org/10.1016/j.gca.2005.04.026.
Thullner, M., Regnier, P., Van Cappellen, P., 2007. Modeling microbially induced carbon degradation in redox-stratified subsurface environments: concepts and open questions. Geomicrobiol J. 24, 139–155. https://doi.org/10.1080/01490450701459275.
Trannum, H.C., Gundersen, H., Escudero-Onate, C., Johansen, J.T., Schaanning, M.T., 2018. Effects of submarine mine tailings on macrobenthic community structure and ecosystem processes. Sci. Total Environ. 630, 189–202. https://doi.org/10.1016/j.scitotenv.2018.02.207.
Urrutia, M.M., Roden, E.E., Fredrickson, J.K., Zachara, J.M., 1998. Microbial and surface chemistry controls on reduction of synthetic Fe(III) oxide minerals by the dissimilatory iron-reducing bacterium Shewanella alga. Geomicrobiol J. 15, 269–291. https://doi.org/10.1080/01490459809378083.
Usman, M., Byrne, J.M., Chaudhary, A., Orsetti, S., Hanna, K., Ruby, C., Kappler, A., Haderlein, S.B., 2018. Magnetite and green rust: synthesis, properties, and environmental applications of mixed-Valent iron minerals. Chem. Rev. 118, 3251–3304. https://doi.org/10.1021/acs.chemrev.7b00224.
Wang, Y., Morin, G., Ona-Nguema, G., Menguy, N., Juillot, F., Aubry, E., Guyot, F., Calas, G., Brown Jr., G.E., 2008. Arsenite sorption at the magnetite-water interface during aqueous precipitation of magnetite: EXAFS evidence for a new arsenite surface complex. Geochim. Cosmochim. Acta 72, 2573–2586. https://doi.org/10.1016/j.gca.2008.03.011.
Watson, I.A., Oswald, S.E., Mayer, K.U., Wu, Y., Banwart, S.A., 2003. Modeling kinetic processes controlling hydrogen and acetate concentrations in an aquifer-derived microcosm. Environ. Sci. Technol. 37, 3910–3919. https://doi.org/10.1021/es020242u.
Younger, P.L., Banwart, S.A., Hedin, R.S., 2002. Mine Water - Hydrology, Pollution, Remediation. 1st ed. Springer Netherlands https://doi.org/10.1007/978-94-010-0610-1.
Zachara, J.M., Fredrickson, J.K., Smith, S.C., Gassman, P.L., 2001. Solubilization of Fe(III) oxide-bound trace metals by a dissimilatory Fe(III) reducing bacterium. Geochim. Cosmochim. Acta 65, 75–93. https://doi.org/10.1016/S0016-7037(00)00500-7.